Optical absorption and applications of the ABO_4 (A=Ca, Pb and B= Mo, W) semiconductors

C. Tablero

Instituto de Energía Solar, E.T.S.I. de Telecomunicación,
Universidad Politécnica de Madrid,
Ciudad Universitaria s/n, 28040 Madrid, SPAIN.
e-mail: ctablero@etsit.upm.es
Tlf: +34 915495700
Fax: +34 915446341

Abstract

Ternary molybdates and tungstates ABO_4 (A=Ca, Pb and B= Mo, W) are a group of materials that could be used for a variety of optoelectronic applications. We present a study of the optoelectronic properties based on first-principles using several orbital-dependent one-electron potentials applied to several orbital subspaces. The optical properties are split into chemical-species contributions in order to quantify the microscopic contributions. Furthermore, the effect of using several one-electron potentials and orbital subspaces is analyzed. From the results, the larger contribution to the optical absorption comes from the B-O transitions. The possible use as multi-gap solar cell absorbents is analyzed.

Keywords: scheelite, electronic structure, optical properties, semiconductors.

1. Introduction

For optoelectronic applications is need to develop new types of materials responding to visible light irradiation. This response is a consequence of the electronic and optical properties. ABO_4 (A = Ca, Pb and B = Mo or W) molybdates and tungstates are two families of materials with interesting luminescence and structural properties.

They have promising applications for solid state lasers [1], scintillators [2-4], electro-optical devices [5], etc.

Calcium and lead molybdates and tungstates are natural minerals. Furthermore, they can be made synthetically. The mineral names associated with these materials are powellite ($CaMoO_4$), scheelite ($CaWO_4$), wulfenite ($PbMoO_4$), and stolzite ($PbWO_4$). The name used to describe the common crystal structure of these materials is scheelite. The scheelite-ABO_4 (A=Ca, Pb and B=Mo, W) crystal structure (Figure 1) is characterized by the tetragonal space group $I4_1/a$ (nº 88). The B atoms are surrounded by four O atoms in an approximately tetrahedral symmetry configuration, and the A atoms are surrounded by eight O atoms in an approximately octahedral symmetry. Many material properties can be associated to the existence of these [BO_4] (Figure 1b) and [AO_8] (Figure 1a) approximate polyhedrons into crystalline structure. The B cation tetrahedra (with W or Mo) behave as rigid structural elements with no observed cation-oxygen compression [6]. On the other hand, compression of the eight-coordinated A=Ca polyhedron, is more favorable parallel to *c* than perpendicular to *c* [6].

Despite the promising properties, these materials have not yet reached the device level. Further applications of these materials require a detailed understanding of their electronic and optical properties. First principles are an important and powerful complementary tool, allowing these basic properties which are hardly accessible by experiments to be obtained and quantified. Therefore we examine the structural, electronic, and optical properties of the ABO_4 Calcium and lead molybdates and tungstates using first-principles techniques.

2. Calculations

We have studied the electronic and optical properties using first principles within the density functional formalism [7,8] but with a further extension including an

orbital-dependent one-electron potential (DFT+U method) [9-13] to account explicitly for the Coulomb repulsions not dealt with adequately in standard approaches. The DFT+U results depend on the U value, on the orbital subspace in which U is applied, on the orbital occupation numbers, and on the implementation chosen [10-13]. In this work we use the DFT+U formalism described in references [10,11] with the generalized gradient approximation from Perdew, Burke and Ernzerhof [14] for the exchange-correlation potential, i.e. GGA+U. Furthermore, we use several U values applied to different orbital subspaces. The pseudopotentials adopted are standard Troullier–Martins [15] expressed in the Kleinman–Bylander [16] factorized form. For the valence wave functions a numerically localized pseudoatomic orbital basis set [17] is used.

The scheelite-ABO_4-type structure (space group $I4_1/a$,nº 88), periodic boundary conditions, spin polarization, double-zeta with polarization localized basis sets, and 128 special *k* points in the irreducible Brillouin zone have been used in all results presented in this work.

The optical properties have been obtained from the complex dielectric function

$$e_2(E) \sim \frac{1}{E^2} \sum_{\mu} \sum_{\lambda > \mu} \int d\vec{k} \; [f_{\mu,\vec{k}} - f_{\lambda,\vec{k}}] |p_{\mu\lambda}|^2 \, \delta(E_{\lambda,\vec{k}} - E_{\mu,\vec{k}} - E)$$

using the Kramers-Kronig relationships. Here $E_{\mu,\vec{k}}$ and $f_{\mu,\vec{k}}$ are the single-particle energies and occupations of the μ band at $\vec{k}$ points in the Brillouin zone, and $p_{\mu\lambda}$ are the momentum ($p=i(m/\hbar)[H,r]$) matrix elements between the μ and λ bands at $\vec{k}$ points. Both, the local and non-local parts of the pseudopotentials have been considered in the calculation of the momentum matrix elements.

3. Results and Discussion

The lattice parameters (*a* (Å), *c* (Å)) used for scheelite-$CaWO_4$ [18], stolzite-$PbWO_4$ [18], powellite-$CaMoO_4$ [18,19] and wulfenite-$PbMoO_4$ [18,20] are (5.243,

11.376), (5.450, 12.030), (5.224, 11.430) and (5.431, 12.106) respectively. Figure 1 shows the crystalline structure in the conventional unit cell.

In our study we have used several GGA+U schemes in order to apply the orbital-dependent one-electron potential: U=0 eV, U=5 eV for *d*(B) orbitals, U_{O3B5} (U=3 eV for the *p*(O) states and U=5 eV for the *d*(B) states), and U_{all}=5 eV (U=5 eV for *d*(B), *p*(O) and *p*(A) orbitals). In Table 1 we report the energy band-gap values obtained and the comparison with other data in the literature. We found that U=5 eV, U_{O3B5} and U_{all}=5 eV schemes gave energy band-gap values closer to other data in the literature. Nevertheless, we not only use different GGA+U schemes with the aim of reproducing energy band gaps, but also to analyze the effect in other properties such as optical properties. The comparison with optical properties is more demanding than the energy band gaps and band structure comparisons, because of the optical properties calculations involved, as well as the electronic structure, the occupations and the transition probabilities.

The electronic band-structure for the four ABO_4 materials in several directions of symmetry within the Brillouin zone is plotted in Figure 2. $CaBO_4$ (B=W, Mo) are direct-gap materials with the band edges on the Γ point. For $PbBO_4$ the edge of the valence band (VB) lies in the M → Γ and M→X directions. These VB maxima are approximately 0.1 eV above the VB-Γ point energy. The conduction band (CB) minimum energy lies on the N point. These materials are almost direct on the N point because the difference between the direct N-gap and indirect gaps is less than 0.1 eV, similar to other results in the literature [21, 22]. Therefore a strong direct optical absorption is expected.

For ABO_4 (A=Ca, Pb and B=Mo, W) the edges of the VB and CB are dominated mainly by the combination of the atomic states in the $[BO_4]$ and $[AO_8]$ approximately polyhedrons into the crystalline structure. The geometry around the B sites is approximately tetrahedral. Therefore the *d*(B) states split into d_e(B) (d_{z^2} and $d_{x^2-y^2}$) and d_t(B) (d_{xy}, d_{xz}, and d_{yz}) states whereas the *s*(B) and *p*(B) atomic states have *a* and *t* tetrahedral symmetry respectively. The crystalline wavefunctions with *t* symmetry are formed mainly by the combination of the d_t(B) and p_t(B) states, and the states with *t* symmetry of the neighboring p_t(O) states.

The main differences in band structure between the $CaBO_4$ and the $PbBO_4$ occur mainly near the top of the VB. From an analysis of the projected density of states (PDOS) on atoms and atomic states, the largest contribution to the VB edge is from the p_t(O) states (Figure 3). In the Pb materials, the top of the VB has an additional contribution from the *s*(Pb) states. These different compositions of the VB top (~ 1 eV below the VB edge in the Pb compounds) can be observed in the electronic structure (Figure 2) and in the density of states (Figure 3) with all GGA+U schemes used.

The bottom of the CB is characterized by the presence of two sub-bands separated energetically by a small gap. This gap is almost zero (< 0.1 eV) for the Pb compounds in accordance with other theoretical results [21]. The lower sub-band in the CB is dominated mainly by d_e(B)-like contributions, while the upper is dominated by d_t(B)-like contributions.

In order to analyze the potential of these semiconductors for optoelectronic applications, we have obtained the optical absorption coefficients. They are shown in Figure 4 for several GGA+U schemes where the energy scale has been shifted by the respective E_g band gap energies. From Figure, between E_g and E_g+2 eV approximately, the differences in the absorption coefficients for different GGA+U schemes is small.

According to the PDOS results, for the ABO_4 compounds the VB and CB edges are made up mainly from the *p*(O) and *d*(B) states respectively. For the A=Pb materials there is a additional contribution from the *s*(A) states to the top of the VB. Therefore, from an analysis based only on the joint DOS, the high absorption should arise mainly from O-B transitions, and with a lower contribution from the O-A transitions for the A=Pb materials. In this simplified joint DOS analysis the transition probabilities (via momentum operator matrix elements) are not taken into account. In order to check the validity of the simplified joint DOS analyses, and quantify the contributions of the transitions between atoms we are going to split the absorption coefficients into intra- and inter-atomic species transitions. To do so, we need to split the $p_{\mu\lambda}$ momentum matrix elements between the μ and λ bands into diatomic contributions $p_{\mu\lambda} = \sum_A \sum_B p_{\mu\lambda}^{AB}$, where $p_{\mu\lambda}^{AB}$ is the inter-specie component that couples basis set functions on different A and B atom species. If A=B, it represent an intra-species component. As the optical properties depend on the square of the momentum operator matrix elements, the absorption coefficient and other optical properties can be split as $\alpha = \sum_A \alpha^{AA} + \sum_A \sum_{B \neq A} \alpha^{AB}$ + (terms involving three and four different species). Note that the intra-species transitions involve both inter- and intra-atomic transitions. Although for atoms the (intra-atomic) transitions between states with equal angular momentum *l* are forbidden, the inter-atomic transitions between atoms located at different sites can be allowed depending on the system (atomic, molecular, solid) symmetry. The same applies to the inter-species transitions.

In Figure 5 the main inter- and intra-species absorption coefficient components have been represented for several GGA+U schemes. The largest contribution to the AC corresponds to the inter-species B-O transitions. These results indicate that the optical properties are determined mainly by the BO_4 tetrahedron, in particular for A=Ca. The

O-O intra-species contributions are also significant, whereas the A-A intra-species contributions are only significant for A=Pb. The other transitions, not shown in the Figure, have a very low contribution close to band-gap energy. Furthermore, as has already been mentioned, into energy range $E_g < E < E_g+2$ eV the differences between the GGA+U results are small when they are scaled by the band-gap energy. The main differences are in the band-gap energy.

Using the energy gap as criterion, the efficiency of the ABO_4 (A=Ca, Pb and B= Mo, W) single-gap semiconductors is very low because the energy gaps are greater than the optimum for a single gap solar cell (~ 41% at E_g ~ 1.1 eV, and at the highest sunlight concentration=46200 sun, where 1 sun=1 Kw/m^2) [26-29]. However, the efficiency can be increased ~ 77 % [29] using multi-gap solar cells, with optimum gaps larger than for single-gap solar cells [26-29]. For multi-gap solar cells, with intermediate bands (IB) between the VB and the CB of the host semiconductor, the absorption of photons will be more efficient than in conventional single-gap solar cells because both VB-IB and IB-CB transitions allow carrier generation from the VB to the CB in addition to the usual process of generation through the VB-CB transitions.

In order to estimate the potentiality of these materials as multi-gap solar-cell devices, we have obtained the maximum efficiency using a generalized multi-gap model [26-28]. These models assume that any non-radiative recombination is suppressed, carrier mobilities are infinite (no ohmic losses), illumination comes from an isotropic gas of photons, and the cell absorbs all incident photons above the band-gap. Using the band-gap energies obtained with U_{all}=5 eV, the limiting efficiencies of scheelite-$CaWO_4$, powellite-$CaMoO_4$, stolzite-$PbWO_4$ and wulfenite-$PbMoO_4$ are between ~ 33-43 %, ~ 38-51 %, ~ 58-73 % and ~ 53-68 % from double- to quintuple–gap solar cell. In

most cases these values exceed the limits of single-gap solar cell (~ 41%), in particular for the A=Pb compounds.

4. Conclusions

Using first-principles methods we have analyzed the electronic and optical properties of ABO_4 (A = Ca, Pb and B = Mo or W) molybdates and tungstates with the scheelite-crystalline structure using several GGA+U schemes. The main differences in the electronic structure between $CaBO_4$ and $PbBO_4$ occur near the edges of the VB and CB. The largest contribution to the VB top is from the *p*(O) states for all compounds. In the A=Pb materials, the VB top has additional *s*(A) contributions. The bottom of the CB is characterized by the presence of two sub-bands separated energetically by a small gap for the Pb compounds. The lower sub-band in the CB is dominated mainly by d_e(B) states, while the upper is dominated by d_t(B) states.

From the optical property results, the largest contribution to the optical absorption corresponds to the inter-species B-O transitions, and for lower proportion to the O-O intra-species transitions. The A-A intra-species transitions are only significant for A=Pb. Into energy range $E_g < E < E_g+2$ eV the differences between the GGA+U results are small when they are scaled by the band-gap energy. The main variation is in the energy gaps. These materials could have a high potentiality as multi-gap solar cell absorbents because they present large efficiencies that, in most cases, exceed the maximum efficiency of single-gap solar cells.

Acknowledgments

This work has been supported by the National Spanish projects PROMESA (ENE2012-37804-C02-01) and MADRID-PV (S2013/MAE-2780).

References

[1] Wang, Y. G.; Ma, J. F.; Tao, J. T.; Zhu, X. Y.; Zhou, J.; Zhao, Z. Q.; Xie, L. J.; Tian, H. Low temperature synthesis of $CaMoO_4$ nanoparticles Ceram. Int. 2007, 33, 693-695.

[2] Mikhailik, V. B.; Kraus, H.; Miller, G.; Mykhaylyk, M. S.; Wahl, D. Luminescence of $CaWO_4$, $CaMoO_4$, and $ZnWO_4$ scintillating crystals under different excitations J. Appl. Phys. 2005, 97, 1181-1191.

[3] Yoon, J. W.; Ryu, J. H.; Shim, K. B. Photoluminescence in nanocrystalline $MMoO_4$ (M = Ca, Ba) synthesized by a polymerized complex method Mater. Sci. Eng. B-Solid State Mater. Adv. Technol. 2006, 127, 154-158.

[4] Andrade, L. H. C.; Li, M. S.; Guyot, Y.; Brenier, A.; Boulon, G. Optical multi-sites of Nd^{3+}-doped $CaMoO_4$ induced by Nb^{5+} charge compensator J. Phys.-Condes. Matter 2006, 18, 7883-7892.

[5] Yu, P.; Bi, J.; Xiao, D. Q.; Chen, L. P.; Jin, X. L.; Yang, Z. N. Preparation and microstructure of $CaMoO_4$ ceramic films prepared through electrochemical technique J. Electroceram. 2006, 16, 473-476.

[6] R. M. Hazen, L. W. Finger and J.W.E. Mariathasan, High-pressure crystal chemistry of scheelite-type tungstates and molybdates. Journal of Physics and Chemistry of Solids 46, 253–263 (1985)

[7] W. Kohn and L. J. Sham, Self-Consistent Equations Including Exchange and Correlation Effects, Phys. Rev. 140, A1133-A1138 (1965).

[8] J. M. Soler, E. Artacho, J. D. Gale, A. García, J. Junquera, P. Ordejon, and D. Sánchez-Portal, The SIESTA Method for Ab initio Order-N Materials Simulation, J. Phys.: Condens. Matter 14, 2745-2779 (2002), and references therein.

[9] V. I. Anisimov, J. Zaanen, and O. K. Andersen, Band Theory and Mott Insulators: Hubbard U instead of Stoner I, Phys. Rev. B 44, 943-954 (1991); V. I. Anisimov, I. V. Solovyev, and M. A. Korotin, M. T. Czyyk, and G. A. Sawatzky, Density-Functional Theory and NiO Photoemission Spectra, Phys. Rev. B 48, 16929–16934 (1993).

[10] C. Tablero, Representations of the Occupation Number Matrix on the LDA/GGA+U Method, J. Phys.: Condens. Matter 20, 325205 (2008).

[11] C. Tablero, Effects of the Orbital Self-interaction in both Strongly and Weakly Correlated Systems, J. Chem. Phys. 130, 054903 (2009).

[12] D. D. O'Regan, M. C. Payne, and A. A. Mostofi, Subspace Representations in Ab initio Methods for Strongly Correlated Systems, Phys. Rev. B 83, 245124 (2011).

[13] M. Grisolía, P. Rozier, and M. Benoit, Density Functional Theory Investigations of the Structural and Electronic Properties of $Ag_2V_4O_{11}$, Phys. Rev. B 83, 165111 (2011).

[14] J. P. Perdew, K. Burke, and M. Ernzerhof, Generalized Gradient Approximation Made Simple, Phys. Rev. Lett. 77, 3865-3868 (1996).

[15] N. Troullier and J. L. Martins, Efficient Pseudopotentials for Plane-wave Calculations, Phys. Rev. B 43, 1993-2003 (1991).

[16] L. Kleinman and D. M. Bylander, Efficacious Form for Model Pseudopotentials, Phys. Rev. Lett. 1982, 48, 1425-1428; D. M. Bylander and L. Kleinman, 4f Resonances with Norm-conserving Pseudopotentials, Phys. Rev. B 41, 907-912 (1990).

[17] O. F. Sankey and D. J. Niklewski, Ab initio Multicenter Tight-binding Model for Molecular-dynamics Simulations and Other Applications in Covalent Systems, Phys. Rev. B 40, 3979-3995 (1989).

[18] R. M. Hazen, L. W. Finger, J.W. E. Mariathasan, High-pressure crystal chemistry of scheelite-type tungstates and molybdates. J. Phys. Chem. Solids 46, 253-263 (1985); A. Zalkin, D. N. Templeton , X-Ray Diffraction Refinement of the Calcium Tungstate

Structure, J. Chem. Phys. 40, 501-504 (1964); M.I. Kay, B.C. Frazer, I. Almodovar , Neutron Diffraction Refinement of $CaWO_4$, J. Chem. Phys. 40, 504-506 (1964).

[19] V.B.Aleksandrov, L.V. Gorbatij, V. V. Iljuhin, Crystal Structure of Powellite $CaMoO_4$, Kristallogr. 13, 512-513 (1967).

[20] J. Leciejewicz, A neutron crystallographic investigation of lead molybdenum oxide, $PbMoO_4$, Z. Kristallogr., 121, 158-164 (1965).

[21] Y. Zhang, N. A. W. Holzwarth, and R. T. Williams, Electronic band structures of the scheelite materials $CaMoO_4$, $CaWO_4$, $PbMoO_4$, and $PbWO_4$, Phys. Rev B 57, 12738-12750 (1998)

[22] Qi-Jun Liu, Zheng-Tang Liu, Li-Ping Feng, and Hao Tian, ISRN Condensed Matter Physics, Volume 2011, Article ID 290741, 7 pages, doi:10.5402/2011/290741.

[23] J. Chen, T. Liu, D. Cao, and G. Zhao, First-principles study of the electronic structures and absorption spectra for the $PbMoO_4$ crystal with lead vacancy, *Physica Status Solidi B*, 245, 1152–1155, 2008.

[24] J. C. Sczancoski, M. D. R. Bomio, L. S. Cavalcante, M. R. Joya, P. S. Pizani, J. A. Varela, E. Longo, M. S. Li, J. A. Andres, Morphology and Blue Photoluminescence Emission of $PbMoO_4$ Processed in Conventional Hydrothermal, J. Phys. Chem. C 2009, 113, 5812-5822.

[25] K. Momma and F. Izumi, "VESTA 3 for three-dimensional visualization of crystal, volumetric and morphology data," *J. Appl. Crystallogr.*, **44**, 1272-1276 (2011).

[26] A. Luque and A. Martí, Theoretical Limits of Photovoltaic Conversion, in Handbook of Photovoltaic Science and Engineering Edited by A. Luque and S. Hegedus, John Wiley & Sons Ltd (2003).

[27] P. Würfel, Physics of Solar Cells. From Principles to New Concepts, 2005 WILEY-VCH Verlag GmbH & Co, KGaA.

[28] M.A. Green, Third Generation Photovoltaics. Advanced Solar Energy Conversion, Springer-Verlag Berlin Heidelberg 2003, 2006.

[29] A. S. Brown and M. A. Green, J. Appl. Phys., 92 (2002) 1329-1336.

List of Tables

	U=0	U=5	U_{O3B5}	U_{all}=5	Other data
SCHEELITE-$CaWO_4$	3.77	4.16	4.45	4.67	4.09[a]
POWELLITE-CaMoO4	3.37	3.72	4.00	4.20	3.41[a]
STOLZITE-PbWO4	2.14	2.46	2.59	2.78	2.96[a]
WULFENITE-PbMoO4	2.43	2.67	2.85	3.13	2.59[a], 2.84[b], 3.17[c]

Table 1: Calculated band-gap energy (eV) using different GGA+U schemes, and literature data: (a) [21], (b) [22], (c) [24].

List of Figures

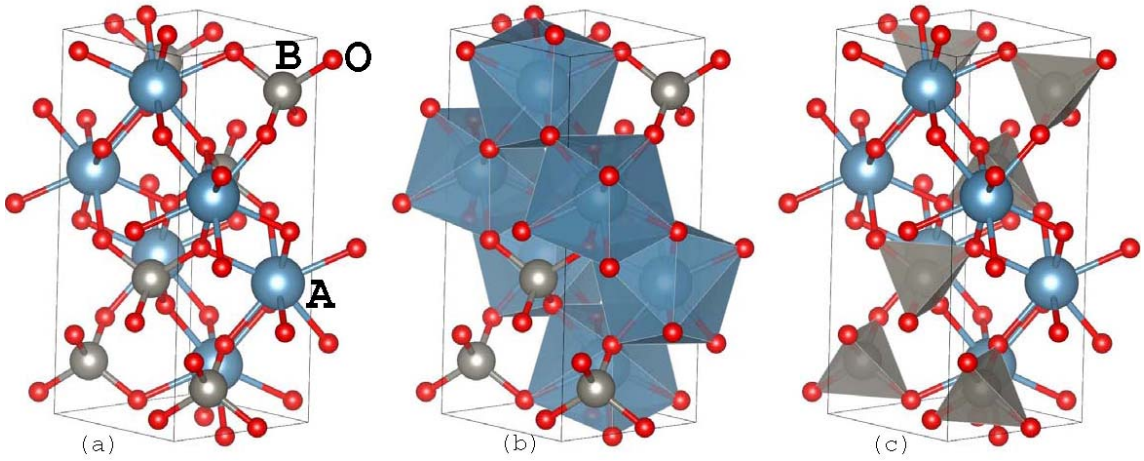

Figure 1

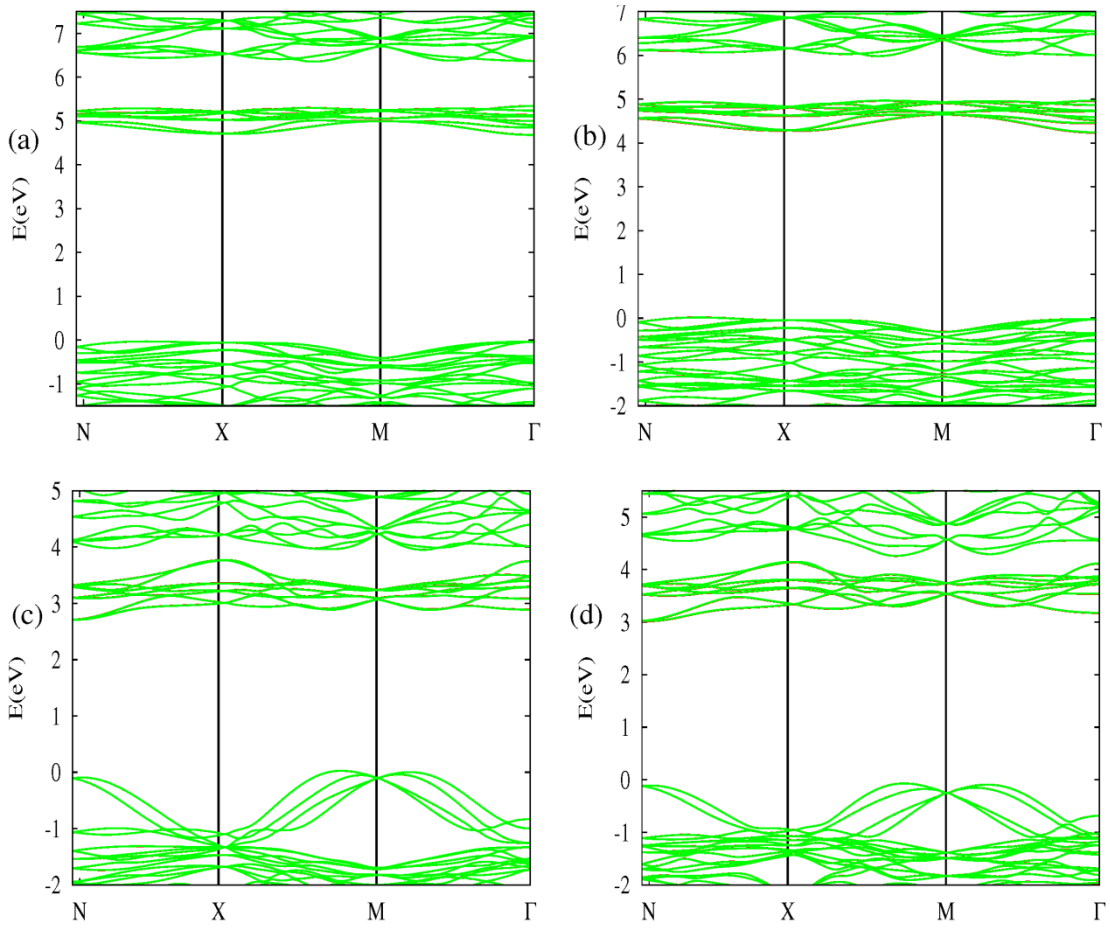

Figure 2

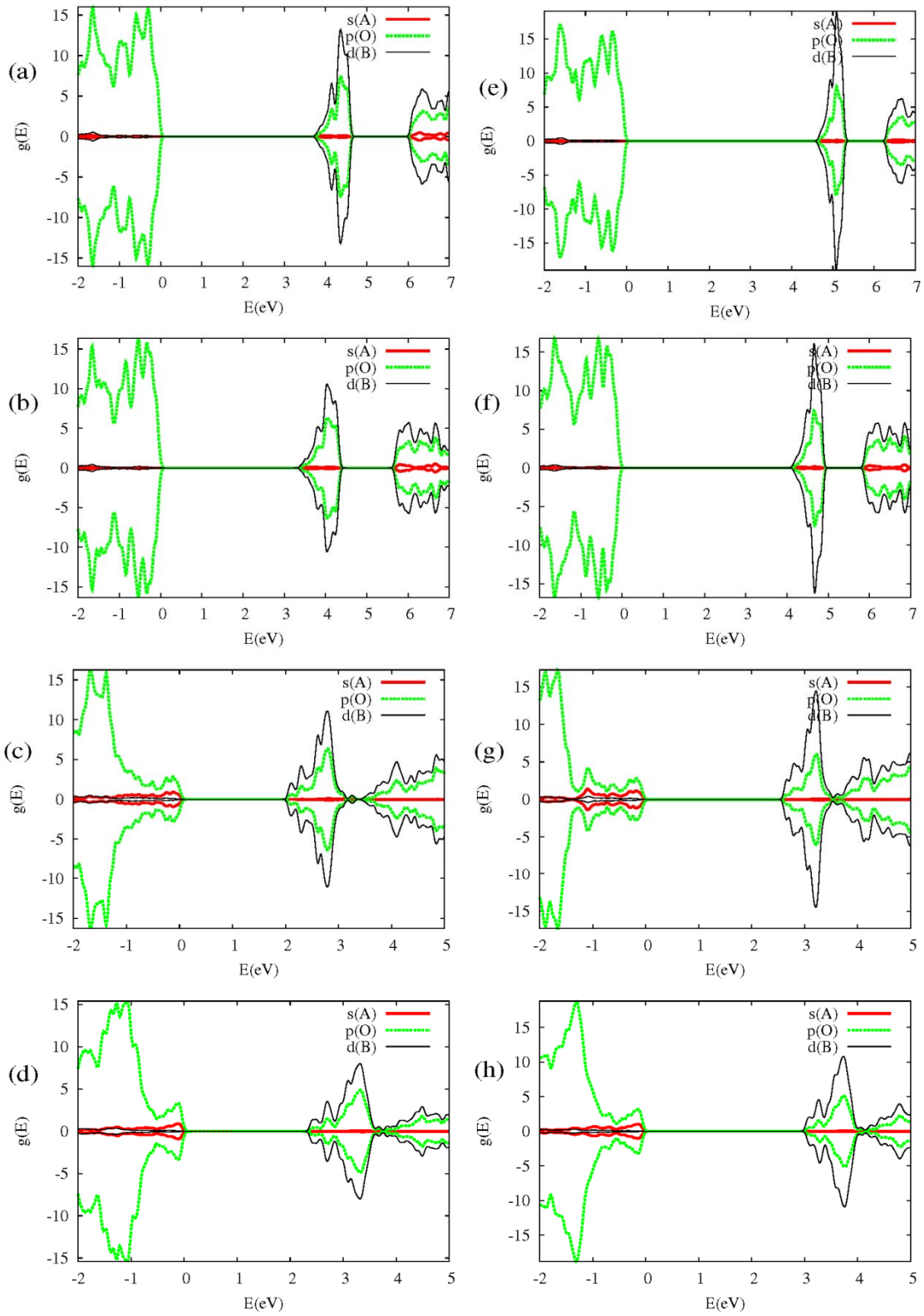

Figure 3

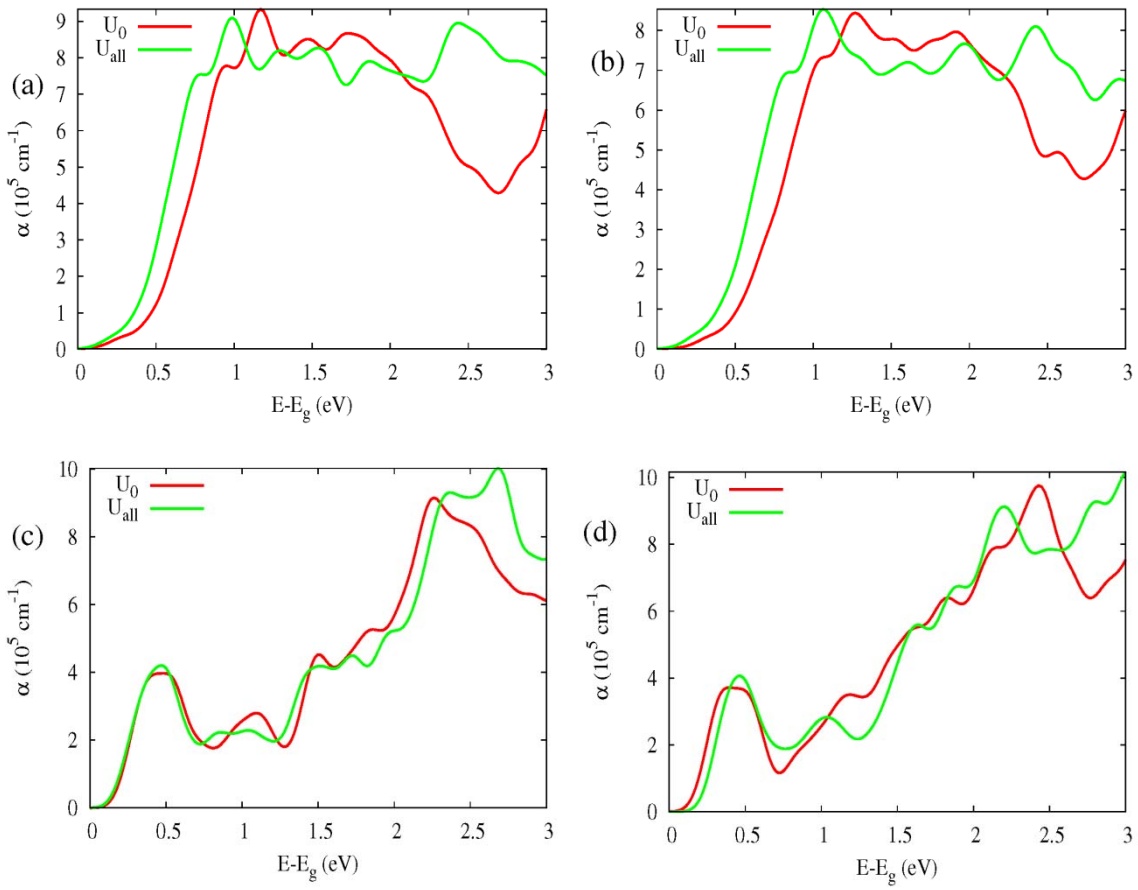

Figure 4

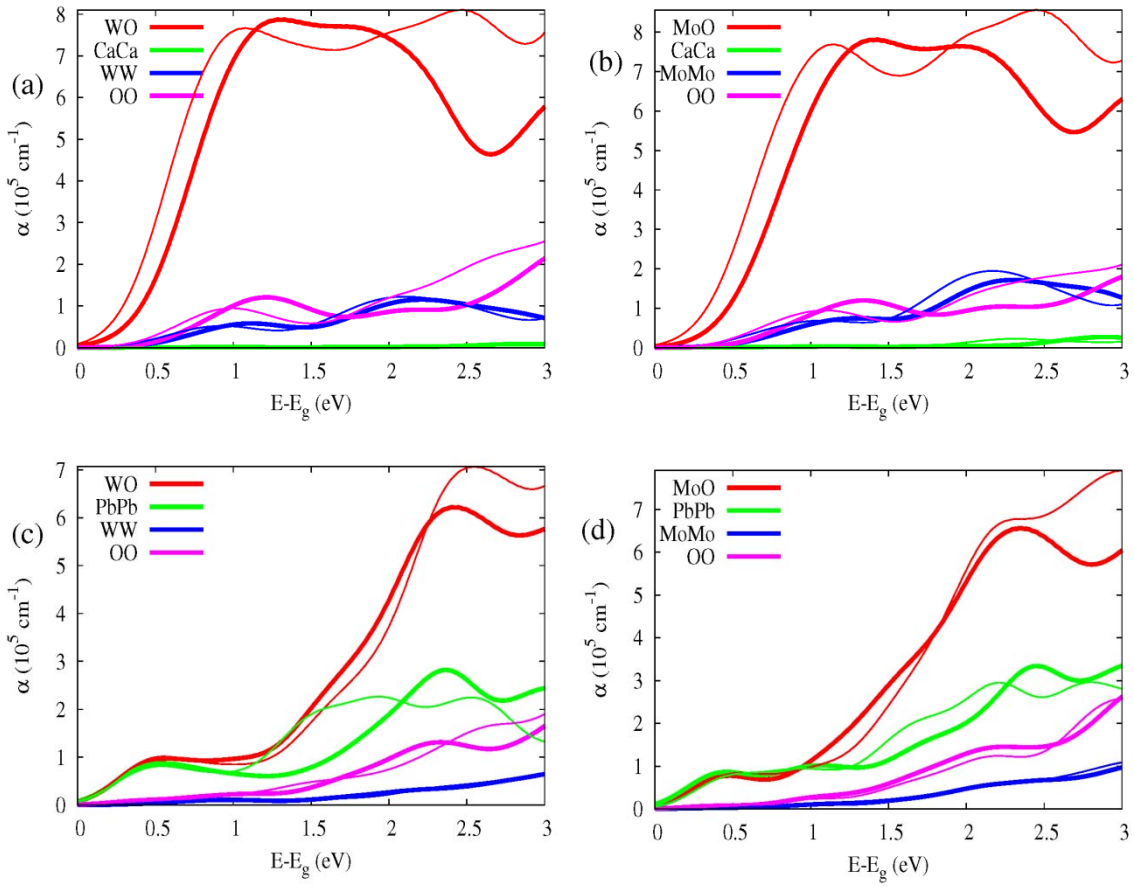
(a)
WO
CaCa
WW
OO
α (10^5 cm^-1)
E-E_g (eV)
(b)
MoO
CaCa
MoMo
OO
α (10^5 cm^-1)
E-E_g (eV)
(c)
WO
PbPb
WW
OO
α (10^5 cm^-1)
E-E_g (eV)
(d)
MoO
PbPb
MoMo
OO
α (10^5 cm^-1)
E-E_g (eV)

Figure 5